Exploring the Effect of Ball Milling on the Physicochemical Properties and Oxygen Evolution Reaction Activity of Nickel and Cobalt Oxides

Sabita Bhandari, Roland Schierholz, Rüdiger-A. Eichel, Ana Laura Luna,*
and Anna Katharina Mechler*

Ball milling is commonly used to reduce catalyst particle size. However, little attention is paid to further changes that ball milling can cause to the rest of the catalysts' physicochemical properties, which can impact their intrinsic catalytic activity. The effect of ball milling on the physicochemical properties of $NiCoO_2$, NiO, CoO, and NiO:CoO mixtures is reported and correlated with their electrochemical oxygen evolution reaction (OER) activity. It is also shown that particle fragmentation is an inherent consequence of ball milling, but some oxides can also experience a phase transformation. In the case of rocksalt-structured CoO, it is partially or entirely transformed to spinel-structured Co_3O_4. Additionally, $NiCo_2O_4$ with a spinel structure can be formed by ball milling NiO and CoO simultaneously (both rocksalt structures), but only in the absence of water. The changes impact the electrochemical activity of the initial oxides. Ball milled $NiCoO_2$ exhibits the highest activity with a mean potential of 1.563 V at 10 mA cm^{-2}, demonstrating the advantage of having Ni and Co in the same structure. Although $NiCo_2O_4$ is also a binary oxide, the results indicate that its metal coordination environment makes it intrinsically less active than $NiCoO_2$ for the OER in alkaline media.

1. Introduction

The oxygen evolution reaction (OER) is a half-cell reaction of water splitting, one of the crucial processes to produce green hydrogen, a versatile energy carrier for replacing fossil fuels and reducing carbon emissions.[1] OER has slow reaction kinetics, making it the bottleneck in water splitting.[1,2] Hence, there is a strong interest in developing highly active OER electrocatalysts. While precious metal oxides such as RuO_2 and IrO_2 are demonstrated to be efficient materials for oxygen evolution in alkaline media, their high cost and scarcity severely limit their applications.[1–3] This has sparked research for earth-abundant low-cost catalysts with high activity. In this context, first-row transition metal oxides are attractive alternatives.

Despite being one of the earliest investigated materials, cobalt oxides (CoO and Co_3O_4) and NiO remain the subject of studies due to their satisfactory OER activity and availability.[4,5] The OER activity of such oxides has been correlated to their active sites' inherent binding energy strength to the different intermediates species (HO*, O*, and HOO*).[4,5] Binary nickel cobalt oxides have also gained attention as a way to profit of from the properties of both NiO and CoO in a single material, pointing them out as promising OER catalysts.[6–8] The activity of such binary oxides is attributed to their high electronic conductivity and a large number of active sites. Besides, it has been observed that OER performance varies depending on the Ni-to-Co ratio,[9,10] but more consensus about the optimal composition is yet to be found. Because of the potential of unary and binary Ni and Co oxides, intensive research efforts have focused on tuning or changing their intrinsic physicochemical properties to yield better OER activity.

Ball milling is a frequently used method to have access to smaller particles and facilitate their subsequent processing, for

S. Bhandari, A. K. Mechler
Electrochemical Reaction Engineering (AVT.ERT)
RWTH Aachen University
Forckenbeckstr. 51, Aachen 52074, Germany
E-mail: anna.mechler@avt.rwth-aachen.de

The ORCID identification number(s) for the author(s) of this article can be found under https://doi.org/10.1002/aesr.202400183.

R.-A. Eichel
Institute of Physical Chemistry
RWTH Aachen University
Aachen 52074, Germany

R. Schierholz, R.-A. Eichel, A. L. Luna, A. K. Mechler
Institute for Energy Technology
Fundamental Electrochemistry (IET-1)
Forschungszentrum Jülich GmbH
Jülich 52425, Germany
E-mail: a.luna.barron@fz-juelich.de

A. K. Mechler
JARA-ENERGY
Aachen 52074, Germany

ADVANCED
SCIENCE NEWS

www.advancedsciencenews.com

ADVANCED
ENERGY & SUSTAINABILITY
RESEARCH
Open Access

www.advenergysustres.com

example, electrode preparation. However, beyond simple particle fragmentation, ball milling may trigger a series of changes in the physicochemical properties of the processed catalytic materials, ultimately impacting their OER activity.[11,12] The changes can be positive or negative. It will depend on the material's properties and the processing conditions.[12,13] In this regard, ball milling can be a door to enhance the catalyst activity, but may also lead to negative effects. Therefore, the changes in physicochemical properties caused by ball milling must be considered when investigating catalysts' OER activity for accurate interpretations.

The essence of ball milling is to generate collision events between powders and balls (i.e., the milling medium), leading to particle fragmentation.[11,12] In planetary-type mills, powders also experience shear and friction.[11] All those events can generate changes of the atomic structure at the particle surface, which might extend to the bulk, resulting in a change or modification of the initial physicochemical properties of the ball milled material. For example, Schüth et al. reported the phase transformation of boehmite (γ-AlOOH) into corundum (α-Al$_2$O$_3$).[14] Similarly, Gajović et al. found that ball milling induced changes in Y$_2$O$_3$ microstructure, introducing distortion of the crystal lattice and oxygen vacancies in the cubic phase.[15] Examples like those emphasize what was mentioned above: the catalysts' property changes caused by ball milling need to be considered for robust OER electrochemical studies. This becomes even more important when two different materials are ball milled together, because ball milling events could also promote chemical reactions between such materials. Indeed, this is why ball milling is currently facing a renaissance as a mechanochemical synthesis method with the advantage of being simple, scalable, and ecofriendly.[11] Various binary oxides have been directly synthesized by this mechanochemical method, such as CoFe$_2$O$_4$[16] and BaFe$_{12}$O$_{19}$.[17] So far, binary oxides have been mechanochemically synthesized using metallic salts as raw materials. However, it remains open whether one can synthesize binary metal oxides by simply ball milling their corresponding unary oxides together. If this were so, ball milling could offer a straightforward and scalable way to synthesize oxides. It would also reaffirm the power of ball milling to change materials' physicochemical properties. Certainly, there is a need to explore what ball milling does to metal oxides when they are processed and how it affects their properties to catalyze OER. This understanding can further contribute to the progress of the development of efficient, cost-effective OER catalysts.

Herein, we investigate the effect of ball milling on the physicochemical properties of NiO, CoO, and NiCoO$_2$ oxides and correlate them with their OER activity. We also elucidate, if mechanochemical reactions between NiO and CoO oxides can occur when they are ball milled together to deliver binary oxides. The non- and ball milled catalysts were characterized by nitrogen gas sorption, X-ray diffraction (XRD), scanning electron microscope (SEM), and X-ray photoelectron spectroscopy (XPS). Cyclic and linear sweep voltammetry were used to assess the OER activity of the oxides in alkaline media. For comparison, the samples were also mixed using a conventional mortar and pestle, a less-intensive energy process than ball milling. Our research reveals that while grinding powders in a mortar causes negligible changes in the physical properties of the processed catalysts, ball milling can provoke not only particle fragmentation, but also partial or full phase transformation in the case of CoO, or even chemical reaction between NiO and CoO, forming spinel NiCo$_2$O$_4$. The investigated oxides' ability to catalyze electrochemical oxygen generation was substantially changed by ball milling.

2. Results and Discussion

2.1. Characterization

In most cases, ball milling is used to decrease the particle size and hence increase surface area. Therefore, as a first assessment, the Brunauer–Emmett–Teller (BET) surface areas are accessed by nitrogen gas sorption, as shown in **Table 1**. The catalysts prepared by dry ball milling exhibited a larger BET surface area (26–42 m^2 g^{-1}) than those processed by conventional milling and the initial commercial oxides. This surface area increase indicates a reduction in catalyst particle size during ball milling. The difference in the resulting specific surface areas between the two mechanical approaches is due to the energy input in milling, which is substantially higher in ball milling than in conventional milling. Generally, high-impact energy gives access to particle size reduction, consequently increasing the specific surface area.[11] Despite the benefits of the high-impact energy of ball milling on particle fragmentation, its effectiveness depends on the mechanical properties of the powders. It has been reported that soft metal oxides might undergo agglomeration due to so-called cold welding.[14] To prevent agglomeration, process control agents such as water, aliphatic alcohols, and stearic acid are commonly used.[11,14,18] We selected water instead of

Table 1. BET specific surface area of commercial NiO, CoO, and NiCoO$_2$ powders and NiO:CoO (50:50) mixtures before and after their mechanical processing by both conventional and ball milling for 4 h at 400 rpm. For wet ball milling, 0.544 µL water per mg of catalyst powder was added. BET mean values with standard deviations. The symbol (*) indicates that the samples were measured only one time.

	BET specific surface area [m^2 g^{-1}]			
–	Unprocessed (initial)	Conventional milling (CM)	Ball milling (BM)	
			Without water (dry)	With water (wet)
NiO:CoO (50:50)	–	18 *	38*	46.5*
NiO	2.0 ± 0.7	2.0 ± 0.9	25.8 ± 0.4	41.7*
CoO	11.5 ± 0.5	15.0 ± 0.3	29.9 ± 0.1	69.8 ± 0.3
NiCoO$_2$	17.8*	13.4 ± 1	42.0 ± 0.2	46.9*

**ADVANCED
SCIENCE NEWS**

www.advancedsciencenews.com

**ADVANCED
ENERGY & SUSTAINABILITY
RESEARCH**
Open Access

www.advenergysustres.com

organic compounds as the process control agent to prevent any organic residues on the catalysts that could interfere with the electrochemical measurements. We performed ball milling in the presence and absence of water. In general, adding water increased the specific surface of the ball milled catalysts compared to those processed without water. For example, the BET surface area of the CoO catalyst prepared by ball milling without water was about $30 \, m^2 \, g^{-1}$, while it was about $70 \, m^2 \, g^{-1}$ with water.

Figure 1a–c shows the SEM images of the investigated oxides before milling. Remarkable differences can be seen between them. While the particles of NiO_{init} are large and form micrometer-sized entities with square edges, the CoO_{init} exhibits spherical-type particles ($<100 \, nm$), which agglomerate only slightly, forming clusters of submicrometer size. $NiCoO_{2\_init}$ has single cubic particles with sizes $<150 \, nm$. The particle morphology and size of the unprocessed oxides agree with their corresponding BET results (see Table 1). For example, the large particles in NiO_{init} explain its negligible BET area ($2 \, m^2 \, g^{-1}$). The cubic shape of the $NiCoO_{2\_init}$ particles leads to a larger BET area than the spherical CoO ones, though the CoO particles are smaller. When commercial oxides were ball milled with water, their particles were fragmented into finer entities, as Figure 1d–f shows. The clearest example was NiO_{wet_BM}, reducing the particle

size from micrometer to submicrometer (Figure 1d). In the case of CoO_{wet_BM} and $NiCoO_{2wet\_BM}$, more individual particles are observed with little difference in the shape.

SEM images of NiO:CoO catalysts are shown in Figure 1g,h. The $NiO:CoO_{CM}$ (50:50) image displays a mixture of micro- and submicro-sized particles, corresponding to the NiO and CoO used to prepare such a catalyst. No particle changes compared to the initial unary oxides are observed, indicating that milling in an agate mortar does not cause particle fragmentation. As in the case of individual oxides, ball milling NiO and CoO together in presence of water causes a clear reduction of particle size (Figure 1h). In general, when oxides are ball milled without water, small but agglomerated particles are observed, as shown in Figure S1, Supporting Information.

All the samples were analyzed using energy-dispersive X-ray spectrometry (EDX) and the results are summarized in Table S2, Supporting Information. The elemental analysis revealed the presence of Ni, Co, O, and C. The carbon signal is attributed to the carbon tape used for mounting the samples. Traces of Zr were observed only in CoO_{wet_BM} and NiO_{wet_BM}, likely originating from the ZrO_2 milling balls and vessels.

We performed XRD measurements to investigate whether conventional milling and ball milling led to phase changes in
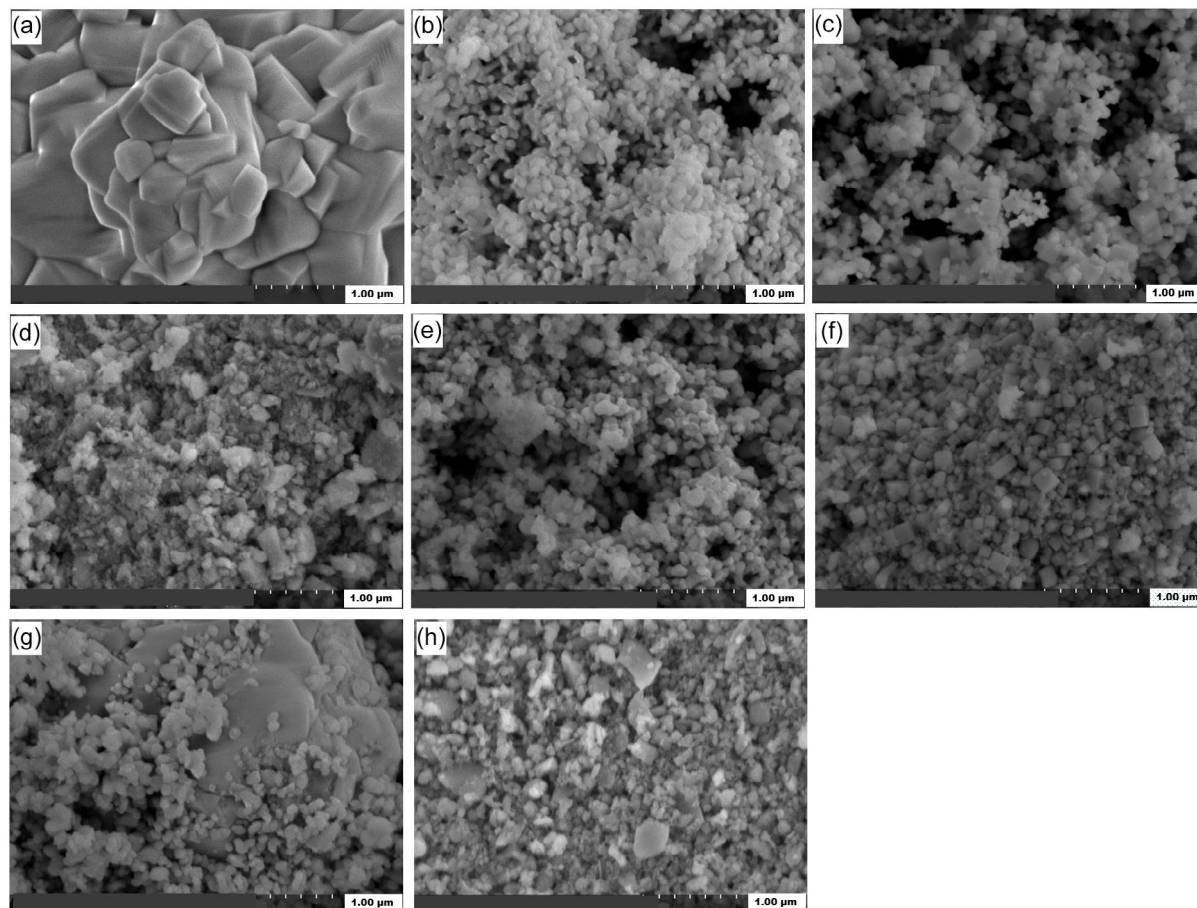

Figure 1. SEM images of commercial oxides and NiO:CoO mixtures before and after conventional milling (CM) or ball milling with water (wet_BM). a) NiO_{init}; b) CoO_{init}; c) $NiCoO_{2\_init}$; d) NiO_{wet_BM}; e) CoO_{wet_BM}; f) $NiCoO_{2\_wet\_BM}$; g) $NiO:CoO_{CM}$ (50:50); h) $NiO:CoO_{wet\_BM}$ (50:50). All figures obtained at the same magnification of 50 k and scale bar corresponds to 1 μm.
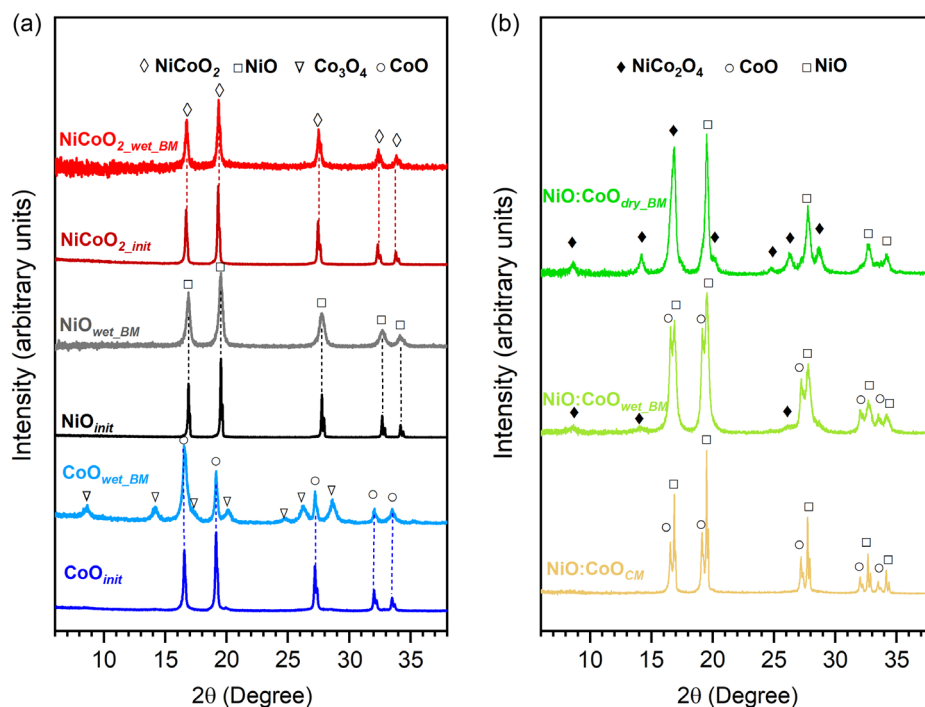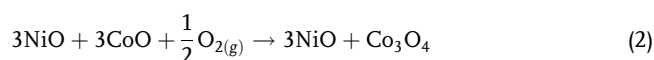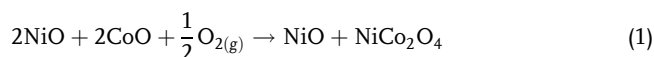
Figure 2. Phase identification of representative samples. XRD of a) commercial NiO, CoO, and $NiCoO_2$ powders before and after ball milling (BM) in the presence of water b) NiO:CoO (50:50) powders prepared by conventional milling and ball milling.

our samples. **Figure 2**a shows the XRD diffractograms of the commercial oxides before and after ball milling in the presence of water, while those of dry ball milled samples are presented in Figure S2, Supporting Information. The XRD patterns of the unprocessed NiO_{init} and CoO_{init} powders agree with the NiO and CoO rocksalt structure (ICSD# 9865 and 9866).[19] $NiCoO_{2\_init}$ shows reflections with positions between pure NiO and CoO, indicating a solid-solution state (according to Vegard's law)[20,21] with a rocksalt structure, confirming the $NiCoO_2$ phase. On the other hand, ball milled samples' diffractograms display broader peaks, indicating crystallite size reduction due to particle fragmentation. Ball milling provoked crystallite size reduction in NiO and $NiCoO_2$ samples, while in CoO, it also led to a partial phase transformation into Co_3O_4 (ISCD# 36 256).[22] Interestingly, when CoO powders are ball milled without water, they undergo complete phase transformation (Figure S2b, Supporting Information). This is remarkable because the transformation of CoO into Co_3O_4 takes, conventionally, place at 240 °C.[23] With the addition of water the phase transformation is partially suppressed.

Figure 2b shows the XRD patterns of selected NiO:CoO samples prepared by conventional milling and ball milling. The diffractogram of $NiO:CoO_{CM}$ (50:50) and $NiO:CoO_{wet\_BM}$ (50:50) displays reflections corresponding to NiO and CoO with a rocksalt structure, indicating that such samples are simple physical mixtures. Conversely, when NiO:CoO samples are ball milled without water, the CoO reflections disappear while new reflections arise. Peaks corresponding to the NiO phase are also observed. The new reflections can be attributed to either Co_3O_4 or $NiCo_2O_4$ phases, which have similar XRD patterns since such

oxides are isostructural. Co_3O_4 or $NiCo_2O_4$ are the two possible oxides that can be formed when NiO and CoO are ball milled simultaneously, as Equation (1) and (2) illustrate. We refined the corresponding XRD pattern to distinguish between the two possible oxides. Details about the refinement are presented in supporting information in Figure S3 and Table S3. The crystalline parameters, Bragg position, and percent phase concentration (48:52 for $NiCo_2O_4$:NiO) obtained in the refinement of NiO:CoO_{dry_BM} (50:50) indicate the formation of $NiCo_2O_4$ spinel oxide. This is important because it shows that binary oxides can be produced by ball milling (without water) from unary oxides (NiO and CoO, in our case).

$$2NiO + 2CoO + \frac{1}{2}O_{2(g)} \rightarrow NiO + NiCo_2O_4 \quad (1)$$

$$3NiO + 3CoO + \frac{1}{2}O_{2(g)} \rightarrow 3NiO + Co_3O_4 \quad (2)$$

Overall, the XRD results revealed three significant findings. First, milling powders in a mortar does not cause a phase change in the metal oxide particles investigated. Second, dry ball milling can result in substantial phase changes or mechanochemical reactions between CoO and NiO. Third, adding water to ball milling reduces the energy transfer during milling impact, preventing or decreasing phase transformations or reactions between oxides.

XPS characterization was performed to elucidate the electrocatalysts' surface composition and chemical state. **Figure 3**a shows the Co 2p spectra of CoO, NiO:CoO, and $NiCoO_2$. It has been reported that the Co $2p_{3/2}$ peak binding energy of
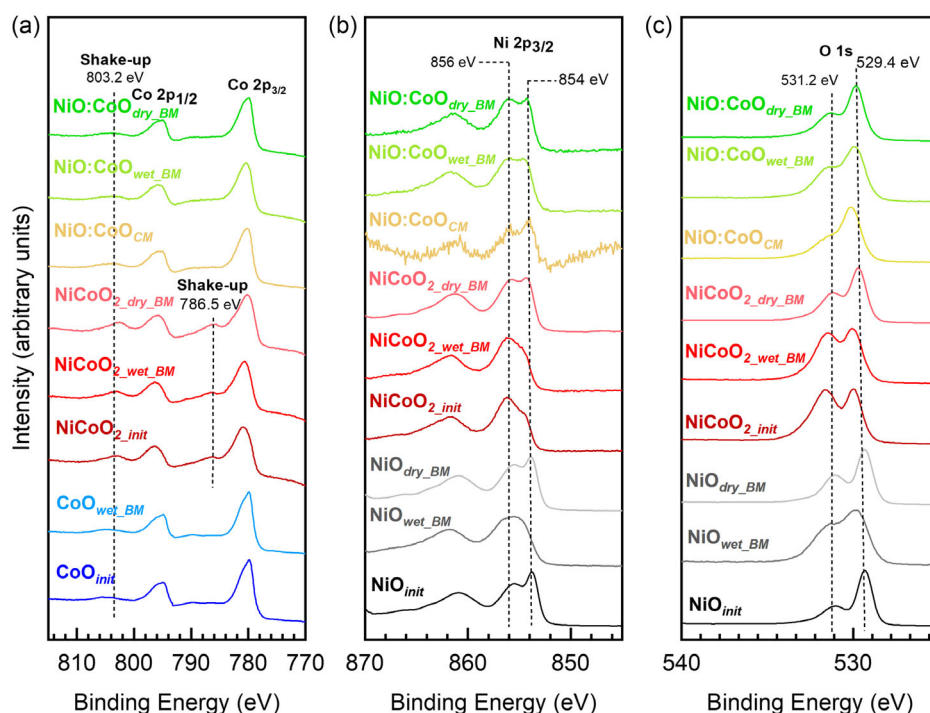
Figure 3. XPS spectra of a) Co 2p, b) Ni 2p, and c) O 1s for the different catalysts as purchased as well as processed by dry and wet ball milling.

various cobalt oxides and hydroxides overlaps, significantly increasing the error in the oxidation state determination.[24] However, differences in the cobalt shake-up peaks provide a more accurate speciation assessment.[25] Therefore, we compared the binding energies of the shake-up peaks rather than those of the Co $2p_{3/2}$ peaks to investigate the cobalt oxidation states. The spectra of the NiCoO$_2$ samples display pronounced shake-up peaks at about 786.5 and 803.2 eV, indicating that its surface is rich in Co^{2+} species. For the CoO and NiO:CoO materials, the peak at about 786.5 eV vanished, and instead only a plateau was observed. The plateau is a hallmark of the coexistence of Co^{2+} and Co^{3+} oxidation states.[24,25] Therefore, the XPS analysis indicates that on the surface of all investigated CoO and NiO: CoO samples, both Co^{2+} and Co^{3+} species are present. The XPS results agree with the crystallographic phases observed in XRD, except for CoO$_{init}$, which displays only XRD peak characteristics of CoO. This discrepancy indicates that the amount of Co^{3+} as Co$_3$O$_4$ in CoO$_{init}$ is very little to be detectable by XRD, which is a bulk technique.

Figure 3b displays the XPS of the Ni $2p_{3/2}$ spectra of NiO, NiCoO$_2$, and NiO:Co samples. The Ni $2p_{3/2}$ structures display two peaks (at ≈854 and ≈856 eV) related to two final states but with different ratio intensities. The first peak (at ≈854 eV) is known as a local screening and is usually assigned to Ni^{2+}, while the second peak, located at ≈856 eV, is known as nonlocal screening and has contributions from surface states.[24,26,27] The ratio intensity between these two peaks differs between each set of samples. For NiO samples the intensity of the surface state peak relative to the Ni^{2+} one is as follows: NiO$_{wet\_BM}$ > NiO$_{dry\_BM}$ > NiO$_{init}$. NiCoO$_2$ samples, on the other hand, display a predominant surface state peak. The intensity of

this peak is reduced after ball milling, especially without water. For the ball milled NiO:CoO, their state surface peaks are as intense as their Ni^{2+} ones. To elucidate the origin of the surface states, we analyze the O 1s XPS spectra shown in Figure 3c. The intensity of the hydroxyl peak (at ≈531.2 eV) changes in the same fashion as the surface state peak in their corresponding Ni $2p_{3/2}$ spectrum, consequently indicating that the surface states in all the samples are related to hydroxyl groups.

To better understand the origin of the hydroxyl groups, the Ni LMM Auger spectra were analyzed. Biesinger et al. demonstrated that NiO, Ni(OH)$_2$, and NiOOH exhibit remarkably different Ni LMM spectra that help with speciation.[28] The Ni LMM spectra reported by Biesinger et al. are presented in **Figure 4**a for a facile comparison. The Ni LMM spectra of the NiO samples correspond indeed to NiO (Figure 4b). The increase of the hydroxyl peak in those samples can be explained by environmental hydroxylation, which naturally occurs in oxides when exposed to the atmosphere. It is further promoted by particle fragmentation due to the increase in the specific surface area. The Ni LMM spectra of NiCoO$_{2\_init}$ and NiCoO$_{2\_wet\_BM}$ show a slight slope between 850 and 842 eV, suggesting a small amount of Ni(OH)$_2$ in addition to NiO. However, for NiCoO$_{2\_dry\_BM}$ the slope is attenuated, resembling NiO more (Figure 4c). This suggests that dry ball milling reduces Ni(OH)$_2$ to NiO in NiCoO$_{2\_dry\_BM}$, which corresponds well with the intensity decrease of the hydroxyl peak (at ≈531.6 eV). Regarding NiO: CoO samples, their Ni LMM spectra indicate the presence of both NiO and Ni(OH)$_2$ (Figure S4, Supporting Information). Overall, the XPS analysis of the Ni $2p_{3/2}$ spectra demonstrates that nickel is present as Ni^{2+}, mainly forming NiO, but for some samples Ni(OH)$_2$ as well. While ball milling does not change the
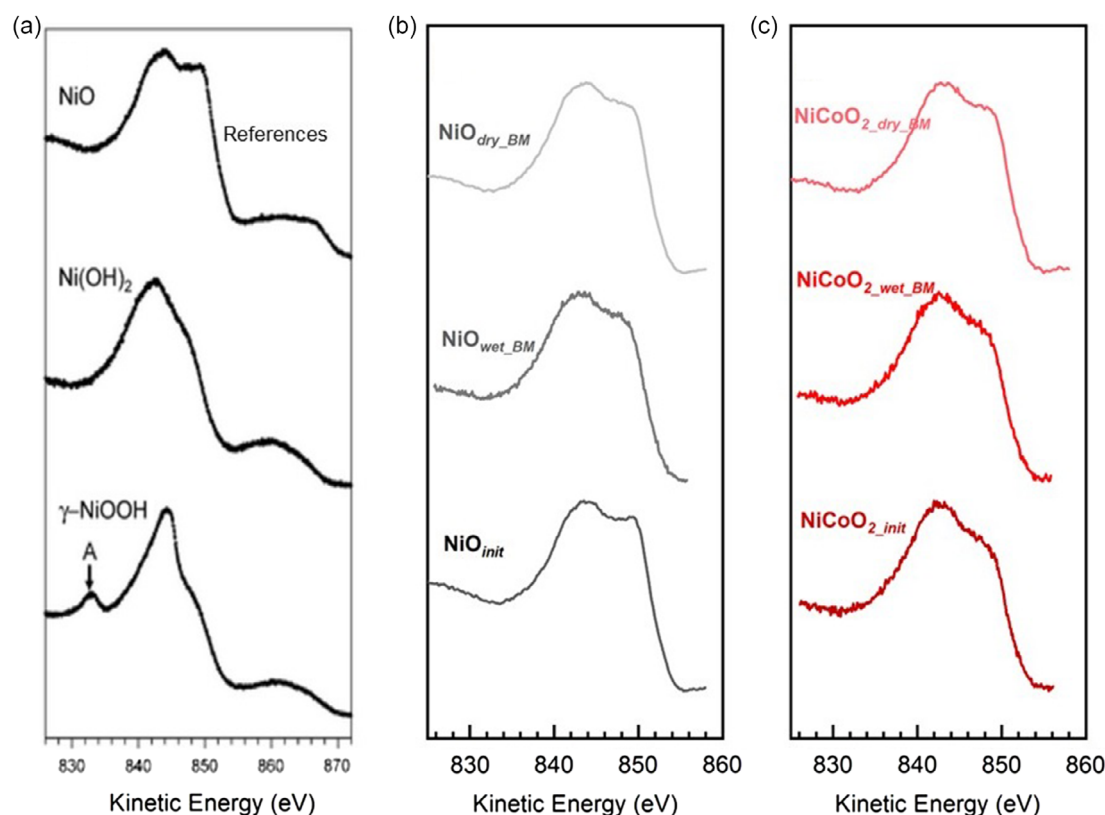
Figure 4. Ni LMM Auger regions of a) reported references (reprinted from ref. [28] with permission from the Royal Society of Chemistry) to compare with the spectra of the herein investigated b) NiO and c) $NiCoO_2$, each as purchased as well as after wet and dry ball milling.

nickel oxidation state, it influences the content of hydroxyls on the surface.

2.2. Electrochemical Characterization

2.2.1. Analysis of CV Peaks

To better understand the changes ball milling causes on the catalysts and how such changes impact their OER activity, features observed in cyclic voltammetry measurements are correlated to the physical and chemical characterization of the catalysts.

NiO, CoO, and $NiCoO_2$ Catalysts: **Figure 5**a shows conditioning cyclic voltammograms (CVs) of commercial NiO before and after ball milling. The three samples exhibit single anodic and cathodic redox peaks attributed to the Ni^{2+}/Ni^{3+} redox couple, confirming that ball milling did not change the Ni^{2+} oxidation state in the sample. However, the redox peaks of the ball milled samples are more intense and shift to higher potentials than those of the unprocessed NiO. For example, the anodic peak of the NiO_{wet_BM} and NiO_{dry_BM} samples shifts by 0.04 and 0.05 V, respectively, relative to the NiO_{init} one (at 1.35 V). These differences probably reflect the increased hydroxylation of the surface that ball milling induced in NiO samples.

Processing CoO by ball milling provoked a Co^{2+} oxidation state and crystalline phase change, as evidenced in CV traces shown in Figure 5b. The CV curves of CoO_{init} show two anodic

peaks at 1.30 and 1.44 V (and their corresponding cathodic peaks at 1.19 and 1.41 V), related to Co^{2+}/Co^{3+} and Co^{3+}/Co^{4+}, respectively. It is known that the octahedral-coordinated Co^{2+} of CoO can be reversibly oxidized and reduced between Co^{2+} and Co^{4+}. Then, the appearance of both redox couples confirms that CoO_{init} is mainly CoO, which agrees with its XRD and XPS characterization. On the other hand, the CV of CoO_{dry_BM} exhibits only a single anodic (at 1.43 V) and cathodic (at 1.41 V) peak, characteristic of the redox couple Co^{3+}/Co^{4+}, as shown in Figure 5b. CV curves with similar shapes have been reported for Co_3O_4.[29–31] Co_3O_4 has a spinel structure, containing Co^{3+} on octahedral coordination sites and Co^{2+} on tetrahedral coordination.[32,33] The Co^{3+} cation in the spinel's octahedral sites is reported to be responsible for the catalysis of OER, yet Co^{2+} in the tetrahedral sites is relatively inactive.[33,34] Then, the absence of Co^{2+}/Co^{3+} peaks in the CV of the CoO_{dry_BM} catalyst indicates a complete phase transformation from CoO to Co_3O_4 under ball milling (without water). Conversely, CoO_{wet_BM} shows a faint anodic peak at 1.3 V revealing the presence of Co^{2+} on octahedral sites characteristic of CoO. This is consistent with the XRD results, which show CoO and Co_3O_4 phases in the CoO_{wet_BM} catalyst. In general, the obtained CVs clearly reflect the partial or full CoO transformation into Co_3O_4 when the powders are ball milled with or without water, respectively.

The $NiCoO_2$ CVs display a broad anodic and cathodic peak at around 1.28 and 1.13 V, respectively, as shown in Figure 5c.
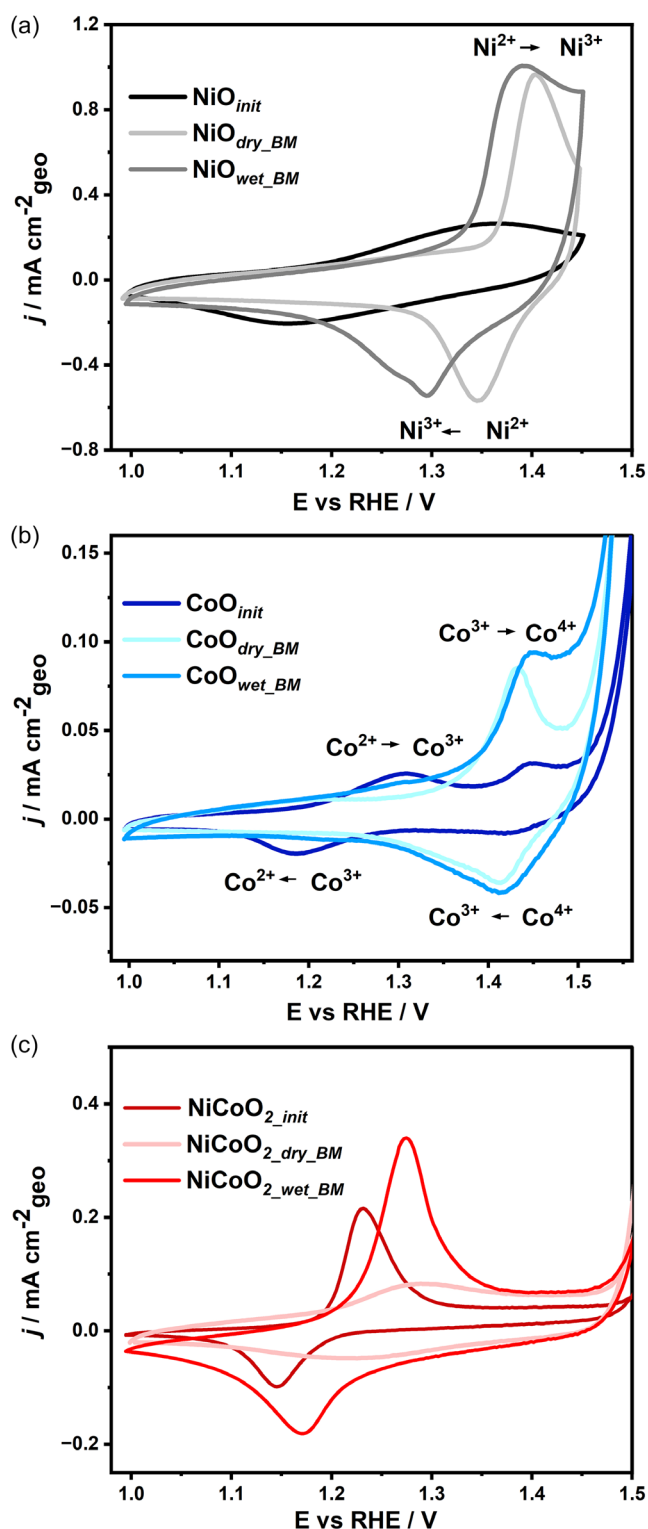
**ADVANCED
SCIENCE NEWS**

www.advancedsciencenews.com

**ADVANCED
ENERGY & SUSTAINABILITY
RESEARCH**
Open Access

www.advenergysustres.com

Figure 5. Comparison of CVs of unprocessed versus ball milled a) NiO, b) CoO, and c) NiCoO$_2$ catalysts in 1 M KOH (binder-to-catalyst ratio: 0.1, loading: 100 µg cm^{-2}, ω: 1600 rpm of RDE).

Similar CV curves have been reported for solid solutions of nickel-cobalt oxide with a Ni:Co atomic ratio of 1:1 (denoted as NiCoO$_2$ or Ni$_{0.5}$Co$_{0.5}$O).[35,36] It agrees with our XRD results, which indicate that the commercial NiCoO$_2$ is a solid solution with a rocksalt structure, where Ni^{2+} and Co^{2+} are coordinated in octahedral sites. These oxidation states match those found in our XPS analysis of the commercial NiCoO$_2$ powders. Therefore, the observed anodic and cathodic peaks can be assumed as the result of the contribution of the redox couples Ni^{2+}/Ni^{3+}, Co^{2+}/Co^{3+}, and Co^{3+}/Co^{4+}. The difference in peak potential is attributed to the surface changes after ball milling which, for NiCoO$_2$ samples, is the decrease of Ni(OH)$_2$.

Mixed NiO:CoO Catalysts: **Figure 6**a shows the conditioning CVs of NiO:CoO prepared by conventional milling with three NiO:CoO mass ratios (25:75, 50:50, and 75:50). Although NiO:CoO$_{CM}$ catalysts contain NiO, in their CVs, the Co^{2+}/Co^{3+} and Co^{3+}/Co^{4+} peaks characteristic of CoO are mainly observed. As the CoO amount increases in the catalysts, the Co^{2+}/Co^{3+} and Co^{3+}/Co^{4+} peaks become more prominent. Conversely, such redox peaks are attenuated when NiO content dominates, resembling the CV of unprocessed NiO. Importantly, despite the different NiO:CoO mass ratios, the redox peak potentials remain unchanged (without shifting). The potential is an intensive property depending only on the system's energy but not on the amount. Therefore, the same peak potential in the NiO:CoO$_{CM}$ CVs implies that conventional milling caused negligible chemical or physical changes in the NiO and CoO powders to modify their catalytic properties. Accordingly, the XRD, XPS, and BET of these samples demonstrated that NiO and CoO remained virtually unchanged after conventional milling. Thus, the fact that NiO:CoO$_{CM}$ CVs exhibit the same redox peak potential confirms again that such catalysts are physical mixtures.

The conditioning CVs of NiO:CoO prepared by dry ball milling are displayed in Figure 6b. NiO:CoO$_{BM}$ CVs differ considerably from NiO:CoO$_{CM}$ CVs. Such differences reflect the complexity of the catalysts as a result of the ball milling. For example, the resulting NiO:CoO$_{dry\_BM}$ catalyst contains NiCo$_2$O$_4$ generated during its processing and the remaining NiO. Particle fragmentation also influenced the NiO:CoO$_{BM}$ CVs. Consequently, the intrinsic complexity of the NiO:CoO$_{BM}$ CVs makes their redox peak assignment difficult. But it is pertinent to point out that the redox peaks appear at different potentials when the NiO:CoO ratio varies, indicating that the overall changes introduced by ball milling alter their electrochemical properties, too.

2.2.2. OER Activity

Finally, we attempt to find a correlation between the observed structural changes and the OER activity of the different catalysts. For activity determination, linear sweep voltammograms (LSVs) were obtained at 5 mV s^{-1}. The LSV are presented in Figure S5, Supporting Information. From these, the mean potential achieved at 10 mA cm^{-2} was obtained for each catalyst and plotted in **Figure 7** to compare their activity. This is a commonly used metric for investigating electrocatalysts' activities on a laboratory scale.[37] Especial care was taken for the reproducibility of the results, leading to comparable small error bars for rotating disk electrode (RDE) experiments of max. ±5 mV.[38]
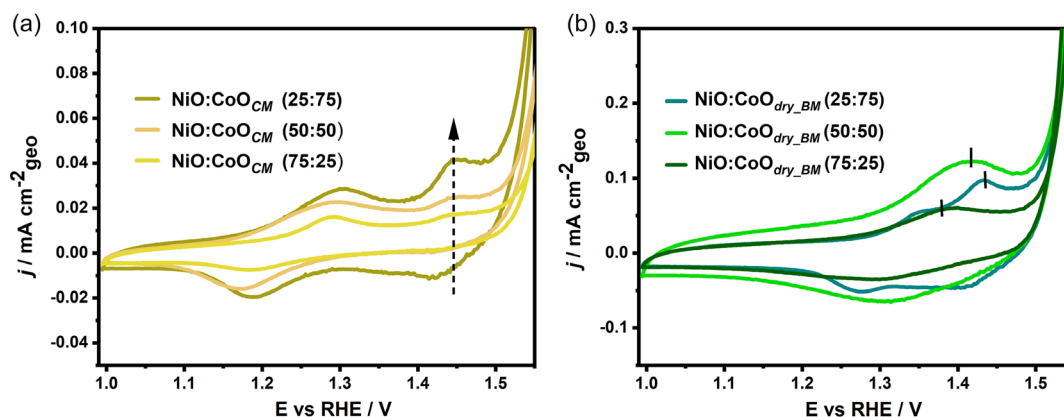
Figure 6. Comparison of conditioning CVs of NiO:CoO catalysts prepared by a) conventional milling and b) dry ball milling.
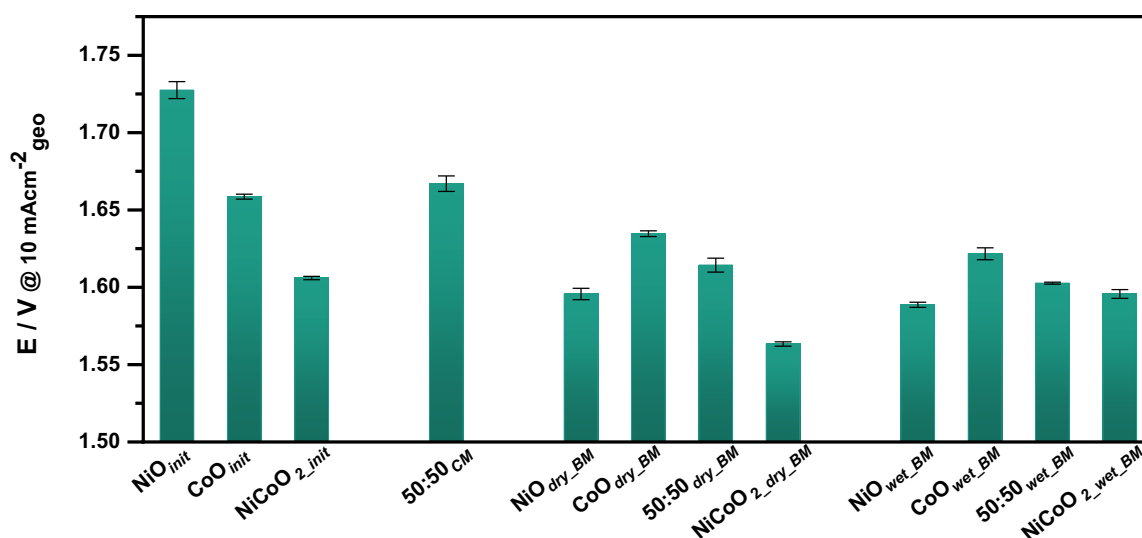

Figure 7. Comparison of mean potential at 10 mA cm$^{-2}_{geo}$ of commercial unprocessed oxides (init), conventionally milled oxide (CM), dry ball milled oxides (dry_BM), and wet ball milled oxides (wet_BM) in 1 M KOH (binder-to-catalyst ratio: 0.1, loading: 100 µg cm^{-2}, ω: 1600 rpm). 50:50 ratios represent NiO:CoO in the binary oxide mixtures.

Activity of NiO, CoO, and NiCoO₂: The comparison of the unprocessed commercial catalysts reveals that the binary oxide $NiCoO_{2\_init}$ is more active, that is, exhibits a lower overpotential than the unary metal oxides, NiO_{init} and CoO_{init}. It highlights the advantages of Ni and Co in the same catalyst. Among the unary oxides, CoO_{init} shows a lower overpotential, which is unexpected as NiO is typically reported to be a more efficient material for oxygen evolution. It is important to note that NiO_{init} particles are micrometer in size, which results in a lower specific surface area ($<2\,m^2\,g^{-1}$) than CoO_{init} ($12\,m^2\,g^{-1}$). The higher the specific surface area, the more active sites are available for water oxidation. Hence, the low activity of NiO_{init} relative to CoO_{init} can be explained by its larger particles.

The activity of the catalysts increases when they are ball milled. In the case of NiO, its efficiency for OER was as follows: $NiO_{wet\_BM} > NiO_{dry\_BM} > NiO_{init}$. This activity trend matches the increase in the BET area, as shown in Table 1. It indicates that particle fragmentation is the change that most influenced the

activity of NiO samples. Notice that after ball milling, NiO becomes a better catalyst than CoO, which is in-line with literature. On the other hand, ball milling CoO also favored its activity. CoO_{wet_BM} and CoO_{dry_BM} are more efficient catalysts than CoO_{init}. The activity of CoO_{wet_BM} is attributed only to particle fragmentation that led to increase its BET surface area of about 5.8 times in comparison to CoO_{init} (see, Table 1). However, in the case of CoO_{dry_BM} its activity cannot be simply attributed to the particle size reduction since ball milling also causes its full transformation to Co_3O_4. The mean potential (1.634 V) of the CoO_{dry_BM} is indeed the activity of Co_3O_4 particles with a BET area of $30\,m^2\,g^{-1}$. Because the BET area between such samples differs, it is difficult to conclude which oxide (Co_3O_4 or CoO) favors OER.

$NiCoO_2$ also exhibited better activity when ball milled. The activity for these three samples is as follows: $NiCoO_{2\_dry\_BM} > NiCoO_{2\_wet\_BM} > NiCoO_{2\_init}$. Notice that the activity trend does not match their specific surface area: $NiCoO_{2\_wet\_BM} > NiCoO_{2\_dry\_BM} > NiCoO_{2\_init}$. Then, the improvement in the

ADVANCED
SCIENCE NEWS
www.advancedsciencenews.com

ADVANCED
ENERGY & SUSTAINABILITY
RESEARCH
Open Access
www.advenergysustres.com

activity of the ball milled $NiCoO_2$ samples cannot be explained only in terms of particle fragmentation. According to the XPS analysis, the $NiCoO_{2\_init}$ surface has $Ni(OH)_2$, which is reduced after ball milling. $NiCoO_{2\_dry\_BM}$ is the sample with the lowest amount of $Ni(OH)_2$ and is also the most active. Thus, the activity improvement in $NiCoO_2$ performance is assigned to both particle fragmentation and $Ni(OH)_2$ reduction.

Activity of Prepared NiO:CoO Catalysts: According to its CV and characterization, $NiO:CoO_{CM}$ (50:50) is a physical mixture of NiO and CoO powders. Despite this, $NiO:CoO_{CM}$ (50:50) showed a significantly lower potential than NiO_{init} and very close to the CoO_{init} mean potential, indicating that the presence of Ni and Co atoms in a catalyst favors the OER reaction rates even though they do not share the same crystalline structure. Nevertheless, having Ni and Co atoms in the same crystalline structure is more powerful as the low mean potential (1.605 V) of $NiCoO_{2\_init}$, which is comparable to $NiO:CoO_{CM}$ (50:50) in terms of specific surface area and Ni:Co atom ratio, indicates.

$NiO:CoO_{dry\_BM}$ also contains a binary oxide, $NiCo_2O_4$. However, its mean potential (1.614 V) is 51 mV above the one higher than that of $NiCoO_{2\_dry\_BM}$, indicating less activity, despite their similar BET areas (difference of only $4\,m^2\,g^{-1}$) and the Ni and Co coexistence in their structure. Such activity difference is explained, in part, by the way in which Ni and Co are arranged in the material. The structural characterization of such samples concluded that $NiCoO_2$ has a rocksalt structure with Ni^{2+} and Co^{2+} at octahedral sites. $NiCo_2O_4$, on the other hand, has a spinel structure, containing Ni^{2+} in octahedral coordination sites and Co^{3+} in both octahedral and tetrahedral coordination. Reported density functional theory calculations have demonstrated that the metal coordination environment in $NiCoO_2$ allows this oxide to have nearly double the concentration of active Ni and Co atoms on its surface than the concentration on the $NiCo_2O_4$ surface.[35] With half of the active atoms exposed on $NiCo_2O_4$ surface, it is reasonable that $NiO:CoO_{dry\_BM}$ performs lower. Thus, although $NiCo_2O_4$ can be formed by dry ball milling, its atom arrangement does not favor the OER, as in the case of $NiCoO_{2\_dry\_BM}$. This highlights that in electrocatalyst activity, the atom arrangement is highly relevant.

To check for significant catalytic changes, the OER curves were further linearized by a Tafel approximation (Figure S6, Supporting Information). Most of the prepared catalyst materials show a slope around $50\,mV\,dec^{-1}$, while CoO_{init}, and $NiO:CoO_{CM}$ show slightly higher slopes about 55 mV. For NiO_{init} a very high slope of about $91\,mV\,dec^{-1}$ can be observed, which can possibly be assigned to the extremely large particle size, leading to an inhomogeneous catalyst layer and possible conductivity issues within the large semiconducting NiO particles. The catalyst with the highest activity in this study, that is, $NiCoO_{2\_dry\_BM}$, also shows the lowest slope with $\approx 34\,mV\,dec^{-1}$.

3. Conclusion

Ball milling has the power to substantially change the original chemical and structural properties of unary and binary Ni and Co oxides to an extent that even new compounds were formed, consequently impacting their OER activity. Ball milling decreases

the particle size, and adding water as a processing agent even favors this effect. Besides, water reduces the possibility of chemical reactions and crystalline phase changes. According to the characterization results, dry ball milling (i) transformed CoO into Co_3O_4, (ii) promoted the reaction between CoO and NiO into $NiCo_2O_4$, and (iii) transformed the $Ni(OH)_2$ present on the $NiCoO_2$ surface into NiO.

For the investigated materials, ball milling enhanced the OER activity of the processed samples. Because water prevents chemical changes, the activity of wet ball milled samples is mainly attributed to particle size reduction. In the case of dry ball milled samples, the activity results from both particle fragmentation and specific chemical changes, the latter having the more significant impact. For example, $NiCoO_{2\_dry\_BM}$ showed a potential 31 mV lower than its analogous $NiCoO_{2\_wet\_BM}$ because surface $Ni(OH)_2$ was reduced after dry ball milling.

This work emphasizes the importance of investigating in detail the overall changes that ball milling might cause to the catalysts to correlate with their activity accurately and ultimately accelerate the development of efficient OER catalyst.

4. Experimental Section

Materials: Nickel cobalt oxide ($NiCoO_2$, 99% trace metals basis), nickel (II) oxide ($NiO \geq 99.995\%$ trace metals basis), cobalt (II) oxide (CoO), and Nafion($\approx 5\%$ in a mixture of lower aliphatic alcohols and water) were purchased from Sigma Aldrich (Merck). Potassium hydroxide (KOH, $\geq 85.0\%$) in pellets and ethanol (ROTIPURAN $\geq 99{,}8\%$) were purchased from Carl Roth. All the chemicals were used as received without further purification.

Electrode Preparation: Commercial NiO, CoO, and $NiCoO_2$ powders were used as raw materials. These metal oxides were ball milled individually with and without water as an additive agent in a planetary ball mill (Fritsch, PULVERISETTE 7). The specific amount of powders (Table S1, Supporting Information) was loaded in a grinding bowl made of stainless steel with an internal ZrO_2 coating, along with ZrO_2 balls of 5 mm diameter. The ball-to-powder mass ratios are summarized in Table S1, Supporting Information. The ball milling vessels were sealed under air. The samples were milled at a rotation rate of 400 rpm for 4 h. When deionized (DI) water was added to the process, a ratio of water to the catalyst of $0.544\,\mu L\,mg^{-1}$ was used. NiO:CoO samples with a mass ratio of 50:50 were prepared by ball milling (BM) commercial NiO and CoO together and applying the abovementioned processing conditions. For comparison, NiO:CoO samples were ground by conventional milling (CM) in an agate mortar and pestled for 10 min.

The unprocessed commercial oxides were labeled as NiO_{init}, CoO_{init}, and $NiCoO_{2\_init}$. When the powders were processed, BM or CM subscripts were used to distinguish between ball milled samples and those processed with conventional agate mortar, respectively. Similarly, the word wet or dry was added to differentiate between samples processed with or without water. So, for instance, NiO_{wet_BM} refers to NiO powders ball milled in the presence of water. On the other hand, NiO:CoO was used to identify mixtures of NiO and CoO. The labeling style applied to refer to the processing method and conditions used was the same as described above. We defined a NiO:CoO ratio mass of 50:50 as the standard ratio. Other NiO:CoO ratios are specified in the manuscript where necessary.

For electrode preparation, the catalysts were dispersed in a solvent mixture to produce a catalyst ink, which was later deposited onto a glassy carbon disk (Metrohm) of 5 mm diameter. The inks comprised 5 mg of catalyst powder in $494.3\,\mu L$ of DI water, $494.3\,\mu L$ ethanol, and $11.4\,\mu L$ of 5 wt% Nafion solution. The ink was sonicated for 15 min, and then $3.92\,\mu L$ were drop coated on the glassy carbon disk (5 mm) of the rotating disk electrode (RDE) resulting in a $100\,\mu g\,cm^{-2}$ catalyst loading. In order to dry the catalyst ink, the glassy carbon disk was rotated at 600 rpm with the disc facing upward.

Electrochemical Characterization: Metrohm RDE and Metrohm potentiostat (PGSTAT204) were used in combination with the NOVA software (Nova 2.1) for the standard electrochemical techniques. Electrochemical measurements were performed in a three-electrode cell with a catalyst-deposited rotating disk electrode as a working electrode, a graphite rod as a counter electrode, and Hg/HgO as the reference electrode (RE) in 1 M KOH at room temperature. The electrode potential collected with Hg/HgO RE was converted to the reversible hydrogen electrode (RHE) scale. All potentials were reported against RHE unless stated otherwise. The electrochemical measurement protocol included conditioning the catalyst via cyclic voltammetry from 1 to 1.45 V at a scan rate of 100 mV s^{-1} at 0 rpm followed by electrochemical impedance spectroscopy (EIS) to determine the solution resistance (i.e., iR-drop). After conditioning and EIS, OER activity was measured by cycling the potential between 1 to 1.8 V at a scan rate of 5 mV s^{-1} at 1600 rpm. The detailed measurement protocol has also been described previously.[38]

Catalyst Characterization: Gas sorption experiments were performed on Micromeritics ASAP 2020 using N_2 at 77 K. The samples were degassed at 100 °C for 12 h prior to the measurement to remove any adsorbed species from the sample surface. The total specific surface area was determined by the multipoint BET method using MicroActive software.

X-ray diffraction (XRD) patterns were recorded on a Panalytical Empyrean diffractometer with Molybdenum Kα radiation and β filter on the diffracted beam side. The generator was operated at 50 kV and 50 A. The angular range from $5 \leq 2\theta \leq 70°$ was scanned stepwise/continuously with 59.69 s/step. Crystalline phase identification was done by comparing the obtained patterns with those reported in the Inorganic Structure Database. Fullprof software was used for X-ray pattern refinement. To improve the fit to the profile parameters, the unit cell and peak profiles were further refined by the full pattern decomposition process for single and overlapping intensities. This was done according to the Le Bail method. The peak profiles were best modeled using a pseudo-Voigt function. The background was estimated and subtracted as a set of points with refinable heights.

A Hitachi Schottky FESEM SU5000 microscope was used to take scanning electron microscopy (SEM) images. The microscope was operated at an accelerating voltage of 5.0 kV and a working distance of 5.8 mm, using secondary-electron mode with a low-angle detector. The SEM was also equipped with an energy dispersive X-ray spectroscopy (EDX) to analyze the elements in the samples. For EDX measurements, the Aztec software from Oxford Instrument was utilized.

X-ray photoelectron spectroscopy (XPS) measurements were performed at the EPSRC National Facility for XPS ('HarwellXPS'), operated by Cardiff University and UCL. The analysis was performed using a Thermo K-Alpha+ XPS fitted with a microfocused monochromatic Al kα X-ray source (1486.7 eV), a spherical sector analyzer, three-multichannel resistive plates, 128 channel delay line detectors. All data was recorded at 72 W with an X-ray beam size of 400×600 μm. Survey scans were recorded at a pass energy of 200 eV, and high-resolution scans were recorded at a pass energy of 40 eV. Electronic charge neutralization was achieved using a dual-beam low-energy-electron/argon-ion source (Thermo Scientific FG-03). The ion gun current was 100 μA. All sample data was recorded at a pressure below 10^{-7} Torr and a room temperature of 294 K. Data was analyzed using CasaXPS v2.3.24. Peaks were fit with a Shirley background prior to component analysis.

Supporting Information

Supporting Information is available from the Wiley Online Library or from the author.

Conflict of Interest

The authors declare no conflict of interest.

Author Contributions

Sabita Bhandari: took care of conceptualization (equal); investigation (equal); and writing the original draft (equal). **Roland Schierholz**: took care of formal analysis (supporting) and writing the review and editing (supporting). **Rüdiger-A. Eichel**: took care of funding acquisition (lead); resources (equal); and writing the review and editing (supporting). **Ana Laura Luna**: took care of conceptualization (equal); investigation (equal); writing the original draft (equal); and writing the review and editing (equal). **Anna Katharina Mechler**: took care of conceptualization (equal); funding acquisition (lead); supervision (lead); and writing the review and editing (equal).

Data Availability Statement

The data that support the findings of this study are openly available in JülichDATA at https://doi.org/10.26165/JUELICH-DATA/QWRPXG.

[1] F. Lu, M. Zhou, Y. Zhou, X. Zeng, *small* **2017**, *13*, 1701931.
[2] F. Song, L. Bai, A. Moysiadou, S. Lee, C. Hu, L. Liardet, X. Hu, *J. Am. Chem. Soc.* **2018**, *140*, 7748.
[3] S. Park, Y. Shao, J. Liu, Y. Wang, *Energy Environ. Sci.* **2012**, *5*, 9331.
[4] M. Bajdich, M. García-Mota, A. Vojvodic, J. K. Nørskov, A. T. Bell, *J. Am. Chem. Soc.* **2013**, *135*, 13521.
[5] I. C. Man, H.-Y. Su, F. Calle-Vallejo, H. A. Hansen, J. I. Martínez, N. G. Inoglu, J. Kitchin, T. F. Jaramilo, J. K. Nørskov, J. Rossmeisl, *ChemCatChem* **2011**, *3*, 1159.
[6] C. Zhu, D. Wen, S. Leubner, M. Oschatz, W. Liu, M. Holzschuh, F. Simon, S. Kaskel, A. Eychmüller, *Chem. Commun.* **2015**, *51*, 7851.
[7] C. G. Morales-Guio, L. Liardet, X. Hu, *J. Am. Chem. Soc.* **2016**, *138*, 8946.
[8] A. Ashok, A. Kumar, J. Ponraj, S. A. Mansour, F. Tarlochan, *J. Electrochem. Soc.* **2018**, *165*, J3301.
[9] G. Wu, N. Li, D.-R. Zhou, K. Mitsuo, B.-Q. Xu, *J. Solid State Chem.* **2004**, *177*, 3682.
[10] J. Chi, H. Yu, G. Li, L. Fu, J. Jia, X. Gao, B. Yi, Z. Shao, *RSC Adv.* **2016**, *6*, 90397.
[11] A. P. Amrute, J. de Bellis, M. Felderhoff, F. Schüth, *Chem. Eur. J.* **2021**, *27*, 6819.
[12] V. Šepelák, S. Bégin-Colin, G. Le Caër, *Dalton Trans.* **2012**, *41*, 11927.
[13] T. Tsuzuki, *Commun Chem* **2021**, *4*, 143.
[14] A. P. Amrute, Z. Lodziana, H. Schreyer, C. Wiedenthaler, F. Schüth, *Science* **2019**, *366*, 485.
[15] A. Gajović, N. Tomasic, I. Djerdj, D. Su, K. Furić, *J. Alloy. Compd.* **2008**, *456*, 313.

[16] Y. Todaka, M. Nakamura, S. Hattori, K. Tsuchiya, M. Umemoto, *Mater. Trans.* **2003**, *44*, 277.

[17] J. Ding, T. Tsuzuki, P. McCormick, *J. Magn. Magn. Mater.* **1998**, *177*, 931.

[18] L. J. Deiner, M. A. Rottmayer, B. C. Eigenbrodt, *J Adv Ceram* **2015**, *4*, 142.

[19] S. Sasaki, K. Fujino, Y. Takéuchi, *Proc. Japan Acad. Ser. B* **1979**, *55*, 43.

[20] L. Vegard, *Z. Phys.* **1921**, *5*, 17.

[21] K. T. Jacob, S. Raj, L. Rannesh, *Int. J. Mater. Res.* **2007**, *98*, 776.

[22] J. P. Picard, G. Baud, J. P. Besse, R. Chevalier, *J. Less-common Met.* **1980**, *75*, 99.

[23] F.-C. Kong, Y.-F. Li, C. Shang, Z.-P. Liu, *J. Phys. Chem. C* **2019**, *123*, 17539.

[24] M. C. Biesinger, B. P. Payne, A. P. Grosvenor, L. W. Lau, A. R. Gerson, R. S. Smart, *Appl. Surf. Sci.* **2011**, *257*, 2717.

[25] D. Gu, C.-J. Jia, C. Weidenthaler, H.-J. Bongard, B. Spliethoff, W. Schmidt, F. Schüth, *J. Am. Chem. Soc.* **2015**, *137*, 11407.

[26] M. A. Peck, M. A. Langell, *Chem. Mater.* **2012**, *24*, 4483.

[27] L. Soriano, I. Preda, A. Gutiérrez, S. Palacín, M. Abbate, A. Vollmer, *Phys. Rev. B* **2007**, *75*, 233417.

[28] M. C. Biesinger, L. W. M. Lau, A. R. Gerson, R. S. C. Smart, *Phys. Chem. Chem. Phys.* **2012**, *14*, 2434.

[29] Y. Wang, T. Zhou, K. Jiang, P. Da, Z. Peng, J. Tang, B. Kong, W.-B. Cai, Z. Yang, G. Zheng, *Adv. Energy Mater.* **2014**, *4*, 1400696.

[30] H. M. A. Amin, H. Baltruschat, *Phys. Chem. Chem. Phys.* **2017**, *19*, 25527.

[31] Q. Liu, Z. Chen, Z. Yan, Y. Wang, E. Wang, S. Wang, S. Wang, G. Sun, *ChemElectroChem* **2018**, *5*, 1080.

[32] H.-Y. Wang, S.-F. Hung, H.-Y. Chen, T.-S. Chan, H. M. Chen, B. Liu, *J. Am. Chem. Soc.* **2016**, *138*, 36.

[33] T. W. Kim, M. A. Woo, M. Regis, K.-S. Choi, *J. Phys. Chem. Lett.* **2014**, *5*, 2370.

[34] Y. Zhang, F. Ding, C. Deng, S. Zhen, X. Li, Y. Xue, Y.-M. Yan, K. Sun, *Catal. Commun.* **2015**, *67*, 78.

[35] X. Sun, J. Sun, L. Guo, L. Hou, C. Yuan, *RSC Adv.* **2020**, *10*, 35611.

[36] K. Fominykh, G. C. Tok, P. Zeller, H. Hajiyani, T. Miller, M. Döblinger, R. Pentcheva, T. Bein, D. Fattakhova-Rohlfing, *Adv. Funct. Mater.* **2017**, *27*, 1605121.

[37] C. C. L. McCrory, S. Jung, J. C. Peters, T. F. Jaramillo, *J. Am. Chem. Soc.* **2013**, *135*, 16977.

[38] M. F. Tesch, S. Neugebauer, P. V. Narangoda, R. Schlögl, A. K. Mechler, *Energy Adv.* **2023**, *2*, 1823.